Field-Calibrated Mechanistic-Empirical Models for Jointed Concrete Pavements

MICHAEL I. DARTER, KURT D. SMITH, AND DAVID G. PESHKIN

Field-calibrated mechanistic-empirical models have been developed for key performance indicators of jointed concrete pavements. Performance data from nearly 500 in-service pavements were used along with mechanistic and empirical variables to develop improved prediction models for joint faulting, slab cracking, joint spalling, and present serviceability rating. The models should prove extremely valuable in checking the performance capabilities of various pavement designs determined by other means and in determining the relative impact of different design variables on concrete pavement performance. However, the models must be used with care and applied judiciously because it is imperative that they not be extended beyond the conditions for which they were developed.

Over the past several years, various models have been developed to predict the performance of in-service concrete pavements. These models can be useful tools in predicting the performance capabilities of a concrete pavement design or in evaluating the impact of different design features on pavement performance. However, there has been some concern about the accuracy of these models and their applicability. A recent FHWA study used performance data from 95 in-service concrete pavements from around the country and evaluated such prediction models as the AASHTO design equation (*1*), the PEARDARP models (*2–4*), the NCHRP 277 (COPES) models (*5*), and the PFAULT faulting models (*6*). The FHWA study found that all of the models were deficient and unable to accurately predict the performance of the in-service concrete pavements (*7*).

Because of the deficiencies of the existing models, improved models were developed using both mechanistic and empirical concepts, which more accurately predict the performance of in-service concrete pavements. To accomplish this, the data from the 95 concrete pavement sections collected under the FHWA study (*7*) were combined with the over 400 concrete pavement sections from the NCHRP 277 (COPES) study (*5*) to allow for a large number of sections and a variety of different pavement designs and design features. Wherever possible, mechanistic variables and functional forms were included. New models were developed for transverse joint faulting (doweled and nondoweled), transverse slab cracking [jointed plain concrete pavement (JPCP) only], transverse joint spalling, and present serviceability rating (PSR). Although there are some limitations with the new models, they are nevertheless believed to be more accurate and more comprehensive than any other prediction models currently available.

ERES Consultants, Inc., 8 Dunlap Court, Savoy, Ill. 61874.

NEW PREDICTION MODELS

Transverse Joint Faulting

Transverse joint faulting is a major distress type that causes loss of serviceability in a jointed concrete pavement. Many jointed concrete pavements have shown serious faulting, which has contributed to the need for expending funds for their rehabilitation.

Design engineers have attempted to reduce faulting through many different ways, including the use of dowel bars, thicker slabs, nonerodible bases, permeable bases, and shorter joint spacing. Many of these attempts have been unsuccessful or only partially successful. Procedures are urgently needed to assist designers in developing joint designs that will experience limited faulting over their service life, yet not result in large initial construction costs due to overdesign.

The data base assembled for this work was greatly expanded and included pavement sections with new design features, such as permeable bases, thick slabs, and the use of dowels in dry climates. There were some areas in which few sections were available, such as doweled slabs in dry-nonfreeze areas (e.g., southwestern United States).

Two prediction models were developed using the combined data bases: one for nondoweled pavements and one for doweled pavements. Because of the mechanisms involved in faulting, it was not useful to combine these two design types into one model. The models were developed using a combination of mechanistic and empirical approaches. The form of the model was based on observations of the development of faulting from field pavements. Key variables that affect faulting were identified from theory and from the data base analysis. Both linear and nonlinear regression techniques were used. Linear regression was used to help identify significant factors in the data base, and nonlinear regression was used to establish the final coefficients on the factors in the form of the model established.

Doweled Concrete Pavements

The mechanistic-empirical faulting model for doweled concrete pavement is as follows:

$$FAULT = ESAL^{0.5280} * [0.1204 + 0.04048 * (BSTRESS1/1000)^{0.3388} + 0.007353 * (AVJSPACE/10)^{0.6725} - 0.1492$$

$$* (\text{KSTAT}/100)^{0.05911} - 0.01868 * \text{DRAIN}$$

$$- 0.00879 * \text{EDGESUP} - 0.00959 * \text{STYPE}] \quad (1)$$

where

FAULT = mean transverse joint faulting (in.);
ESAL = cumulative 18-kip equivalent single axle loads (ESALs) (millions);
BSTRESS = maximum concrete bearing stress using closed-form equation (psi) = $f_d * P * T * [K_d * (2 + \text{BETA} * \text{OPENING})/(4 * E_s * I * \text{BETA}^3)]$;
BETA = $[K_d * \text{DOWEL}/(4 * E_s * I)]^{0.25}$;
f_d = distribution factor = $2 * 12/(l + 12)$;
l = radius of relative stiffness (in.) = $\{E_c * \text{THICK}^3/[12 * (1 - u^2) * \text{KSTAT}]\}^{0.25}$;
E_c = concrete modulus of elasticity (psi) = $14.4 * 150^{1.5} * \text{MR}_{28}^{0.77}$;
I = moment of inertia of dowel bar cross section (in.^{4}) = $0.25 * 3.1416 * (\text{DOWEL}/2)^4$;
THICK = slab thickness (in.);
MR_{28} = concrete modulus of rupture at 28 days (psi);
u = Poisson's ratio, set to 0.15;
P = applied wheel load, set to 9,000 lb;
T = percent transferred load, set to 0.45;
K_d = modulus of dowel support, set to 1,500,000 pci;
BETA = relative stiffness of the dowel-concrete system;
DOWEL = dowel diameter (in.);
E_s = modulus of elasticity of the dowel bar (psi);
KSTAT = effective modulus of subgrade reaction on the top of base (psi/in.);
OPENING = average transverse joint opening (in.) = CON * AVJSPACE * 12 * (ALPHA * TRANGE/2 + e);
AVJSPACE = average transverse joint spacing (ft);
CON = adjustment factor due to base/slab frictional restraint (0.65 if stabilized base, 0.80 if aggregate base or lean concrete base with bond breaker);
ALPHA = thermal coefficient of contraction of portland cement concrete (PCC), set to 0.000006/°F;
TRANGE = annual temperature range (°F);
e = drying shrinkage coefficient of PCC, set to 0.00015 strain;
DRAIN = index for drainage condition (0 if no edge support exists, 1 if edge subdrain exists);
EDGESUP = index for edge support (0 if no edge support exists, 1 if edge support exists); and
STYPE = index for AASHTO subgrade soil classification (0 if A–4 to A–7, 1 if A–1 to A–3).

Statistics:

R^2 = 0.67,
SEE = 0.057 in., and
n = 559 data points.

The bearing stress between the concrete and the dowel was computed using an equation developed by Ioannides et al. (*8*).

The prediction model presented includes many variables that have been shown by theory and field investigations to affect faulting. These variables include repeated heavy traffic loadings, dowel bearing stress (which is greatly affected by dowel diameter), joint spacing, effective k-value, longitudinal drains, edge support from tied PCC shoulders or widened traffic lanes, and type of subgrade.

A sensitivity of the doweled faulting model is shown in Figures 1 and 2. Dowel diameter (for a constant dowel spacing of 12 in.) and provision for subdrainage are observed to be the most critical design factors affecting transverse joint faulting.

Nondoweled Concrete Pavements

The faulting model for nondoweled concrete pavement slabs is as follows:

$$\text{FAULT} = \text{ESAL}^{0.2500} * [0.000038$$

$$+ 0.01830 * (100 * \text{OPENING})^{0.5585}$$

$$+ 0.000619 * (100 * \text{DEFLAMI})^{1.7229}$$

$$+ 0.0400 * (\text{FI}/1000)^{1.9840} + 0.00565 * \text{BTERM}$$

$$- 0.00770 * \text{EDGESUP} - 0.00263 * \text{STYPE}$$

$$- 0.00891 * \text{DRAIN}] \quad (2)$$

where

TRANGE = annual temperature range (minimum average January temperature − maximum average July temperature) (°F);
DEFLAMI = Ioannides' corner deflection (in.) (*8*) $P * (1.2 - 0.88 * 1.4142 * a/l)/(\text{KSTAT} * l^2)$;
a = radius of the applied load, set to 5.64 in. and assuming tire pressure = 90 psi;
BTERM = base type factor = $10 * [\text{ESAL}^{0.2076} * (0.04546 + 0.05115 * \text{GB} + 0.007279 * \text{CTB} + 0.003183 * \text{ATB} - 0.003714 * \text{OGB} - 0.006441 * \text{LCB})]$;
GB = dummy variable for dense-graded aggregate base (1 if aggregate base, 0 otherwise);
CTB = dummy variable for dense-graded, cement-treated base (1 if cement-treated base, 0 otherwise);
ATB = dummy variable for dense-graded, asphalt-treated base (1 if asphalt-treated base, 0 otherwise);
OGB = dummy variable for open-graded aggregate base or open-graded, asphalt-treated base (1 if open-graded base, 0 otherwise);
LCB = dummy variable for lean concrete base (1 if lean concrete base, 0 otherwise); and
FI = freezing index (degree-days).

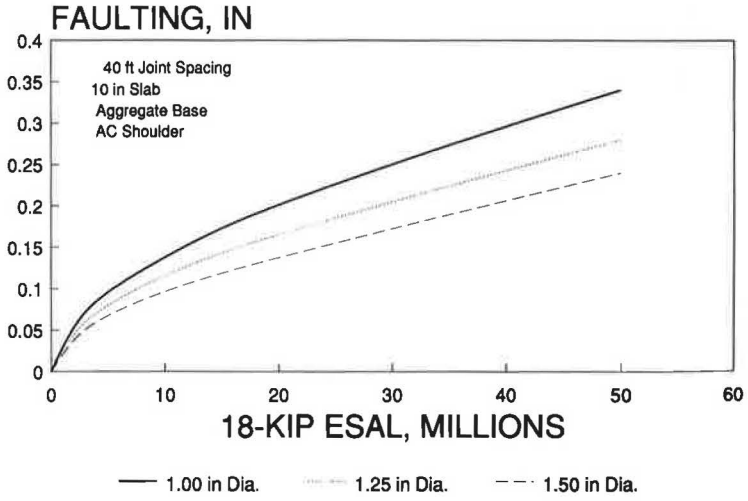

FIGURE 1 Sensitivity of doweled faulting model to dowel diamater.

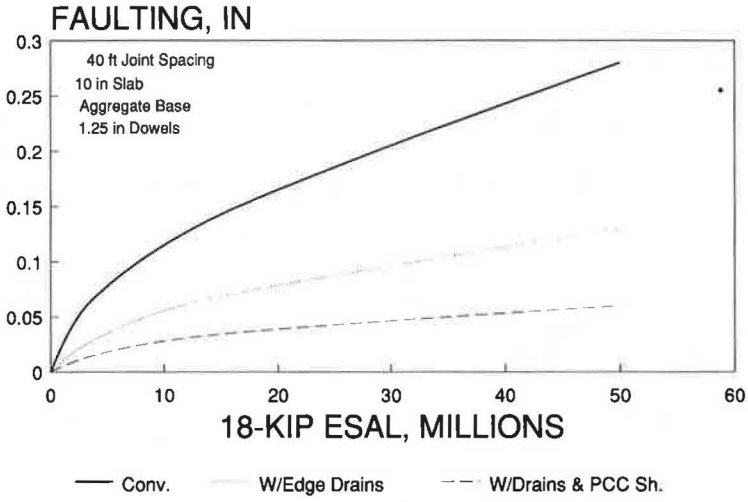

FIGURE 2 Sensitivity of doweled faulting model to drainage and shoulder type.

Statistics:

$R^2 = 0.81$,
SEE = 0.028 in., and
$n = 398$.

The corner deflection used in the nondoweled faulting model was computed using a relationship developed by Ioannides et al. (*8*).

The prediction model presented includes many variables that have been shown by theory and field investigations to affect faulting of nondoweled joints. These variables include repeated heavy traffic loadings, base type, free corner deflection (which is a function of slab thickness and effective *k*-values), joint opening (which is a function of temperature, joint spacing, and slab-base friction), climate, longitudinal drains, edge support from tied PCC shoulders or widened traffic lanes, and type of subgrade.

A sensitivity of the doweled and nondoweled faulting model is shown in Figure 3. Base type, drainage, joint spacing, and ESALs are observed to be the most critical design factors affecting transverse joint faulting.

These mechanistic-empirical models for joint faulting can be used for checking joint designs to determine if the design will prevent significant faulting for the given design traffic, climate, and subgrade soils. Examples of applying this type of model for checking joint designs are given by Heinrichs et al. (*6*).

Transverse Cracking

Transverse cracking in concrete slabs may occur for a number of reasons. Large temperature gradients through the slab, heavy-truck loadings, and shrinkage of the concrete immediately after placement can all produce stresses in the slab that can result in transverse cracking. Once initiated, transverse cracks are entry points for water and incompressibles and can deteriorate further under traffic loadings. The pres-

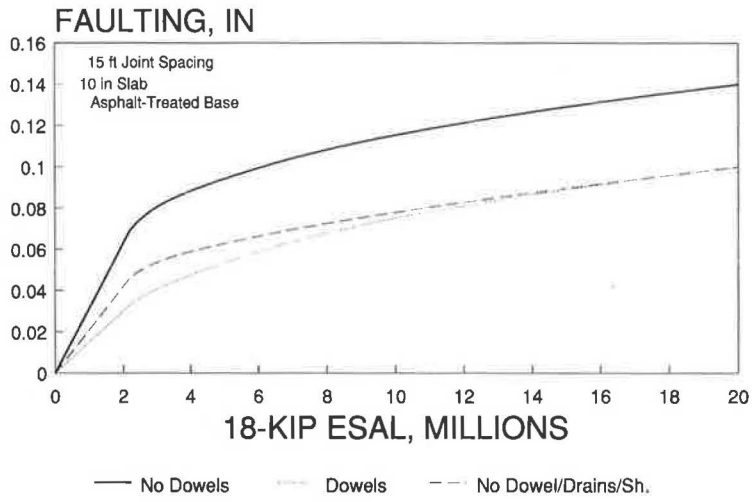

FIGURE 3 Sensitivity of faulting models to dowels, drainage, and shoulder type.

ence of excessive transverse cracking can significantly detract from the overall serviceability of a concrete pavement.

Transverse cracks can occur both in JPCP and in jointed reinforced concrete pavements (JRCP). However, the mechanism influencing their occurrence in each pavement type is different. For example, transverse cracks occurring in JPCP are usually caused by either thermal curling or truck loading (fatigue), whereas transverse cracks occurring in JRCP are generally caused by thermal curling and shrinkage. In fact, JRCP is actually designed to crack. That is, the long joint spacing for JRCP (generally 40 ft or longer) produces excessive thermal stresses that result in transverse cracking. However, the slabs contain reinforcing steel, which is expected to hold the cracks tight. Efforts were concentrated on developing a model for transverse cracking in JPCP.

The model developed was based on a fatigue-consumption approach similar to that used by Darter (*9*). This concept theorizes that a concrete pavement has a finite life and can withstand a maximum allowable number of repetitions, N, of a given traffic loading until a critical proportion of slabs are cracked. Every individual traffic loading applied, n, decreases the life of the pavement by an infinitesimal amount. Theoretically, when $\Sigma n/N = 1$, fracture of 50 percent of the concrete slabs occurs. However, because of the range in variability of materials, traffic loading, and other properties, there is a large variation in fatigue life that results in a distribution around the $\Sigma n/N = 1$ point.

The following paragraphs outline the procedure followed in the development of the JPCP cracking model, using only the 52 JPCP sections from the FHWA study.

Applied n

On the basis of historical traffic data, W–4 tables, and on-site weigh-in-motion (WIM) data, the number of 18-kip ESAL applications was estimated for each JPCP section. However, not all of these loadings were located at the slab edge. Studies have shown that trucks encroach into an edge loading condition (say, within 12 in. of the slab edge) only between 3 and 7 percent of the time (*10*). Thus, it was assumed that an average of 5 percent of the trucks loaded the slab at the critical edge location. However, if a pavement section had a widened outside traffic lane, it was assumed that only 0.1 percent of the truck lane loadings produced an edge loading condition (*10*). The edge loading condition is considered critical for JPCP because this location has the maximum stress in the slab under temperature and traffic loading and will be the point of crack initiation.

For example, if a pavement has endured an estimated 10 million 18-kip ESAL applications, it is assumed that only 5 percent, or 0.5 million, ESAL applications occur at the critical edge location; therefore, $n = 0.5$ million. Similarly, if the pavement has a widened outside traffic lane, only 0.1 percent, or 0.01 million, 18-kip ESAL applications ($n = 0.01$ million) are assumed to occur at the critical edge location.

As the indicator for applied loadings, 18-kip ESAL applications were selected because this quantity is easier to compute than detailed axle load data. Detailed axle load information would provide more accurate results but can often be a tedious and difficult computation; furthermore, reliable axle load data are not always readily available. Additionally, as illustrated in the following paragraphs, a fairly good relation was obtained using the 18-kip ESAL applications.

The load equivalency factors used in estimating ESAL applications are from the AASHO Road Test and are based on serviceability rather than cracking. Therefore, there is some error associated with using ESAL applications as the loading factor in the fatigue analysis. Cracking-based load equivalency factors would undoubtedly provide a better estimate of 18-kip ESAL applications, although nearly all of the loss of serviceability at the AASHO Road Test was due to slab cracking caused by erosion and loss of support.

Allowable N

The maximum allowable number of repetitions, N, is computed using concrete fatigue damage considerations. First, stresses at the concrete slab edge were computed for a com-

bination of traffic loading and thermal curling. These stresses were calculated using equations developed by Darter (*9*). A 9,000-lb wheel load was assumed for the load calculation, and the yearly average thermal gradients presented in Table 1 were assumed for the thermal curling calculation. These thermal gradients are daytime gradients, which represent the critical thermal curling condition when thermal stresses and load stresses are additive. By considering the gradients, the total stress at the slab edge due to loading and thermal curling was determined.

The stress at the slab edge was reduced, however, if tied concrete shoulders were present. Tied concrete shoulders are expected to provide support to the mainline pavement and thereby reduce the magnitude of the critical edge stress. Because the deflection load transfer between the mainline pavement and tied concrete shoulder had been obtained during field testing, the amount of support, or edge stress reduction, could be estimated from Figure 4. This figure provides the equivalent stress load transfer for a given deflection load transfer, and this stress load transfer was used to determine the amount of support (and hence the reduction in the number of 18-kip ESAL applications) provided by the concrete shoulders. For example, if the deflection load transfer efficiency (LTE) for a concrete shoulder is 43 percent, the equivalent stress LTE is approximately 14 percent (only 14 percent of the stress is being transferred). Therefore, because

$$\text{Total stress} = \text{stress}_{\text{loaded}} + \text{stress}_{\text{unloaded}}$$

and

$$\text{Stress LTE} = \text{stress}_{\text{unloaded}}/\text{stress}_{\text{loaded}}$$

then

$$\text{Total stress} = \text{stress}_{\text{loaded}} + \text{stress}_{\text{loaded}} * \text{stress LTE}$$

or

$$\text{Stress}_{\text{loaded}} = \text{total stress}/(1 + \text{stress LTE}) \quad (3)$$

Thus, for this example, the computed (total) edge stress would be multiplied by a factor of [1/(1 + 0.14)], or 0.88.

The stress equations provided by Darter (*9*) require several section-specific design inputs, including slab thickness, composite *k*-value, and slab length. For sections with random slab lengths (e.g., 12, 13, 19, and 18 ft), each slab length was considered individually because the stresses produced on each slab would be different. The percentage of slabs cracked was broken down according to slab length. In this way, there were actually 184 cases representing the 52 JPCP sections.

TABLE 1 YEARLY AVERAGE DAYTIME THERMAL GRADIENTS USED IN CURLING COMPUTATIONS, °F/IN. (*9*)

Slab Thickness, in	Wet-Nonfreeze Climatic Zone	Dry/Wet-Freeze Climatic Zones	Dry-Nonfreeze Climatic Zone
8	1.40	1.13	1.41
9	1.30	1.05	1.31
10	1.21	0.96	1.21
11	1.11	0.87	1.10
12	1.01	0.79	1.00

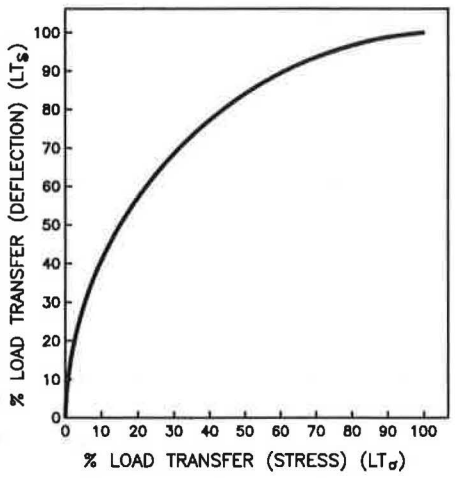

FIGURE 4 Relationship between deflection and stress load transfer.

With the critical stress value calculated for the slab edge, the stress ratio was computed. The stress ratio is defined as the ratio of the edge stress to the 28-day modulus of rupture (third point). This value was then directly entered into the following field-derived fatigue equation:

$$\log_{10} N = 2.13 * (1/\text{SR})^{1.2} \quad (4)$$

where N is the allowable 18-kip applications and SR is the stress ratio (ratio of computed edge stress to 28-day modulus of rupture).

Equation 4 was originally developed for airfield slabs that had been loaded with aircraft gears, but it has shown good results in highway applications (*11*). The curve is very different from those typically derived in laboratory beam testing.

JPCP Cracking Model

With the determination of n and N, cumulative fatigue damage (n/N) was calculated for each JPCP section (or for each individual slab length for JPCP sections with random joint spacing). The base 10 logarithm was taken of each fatigue damage value and plotted against the corresponding percent slabs cracked, as shown by the individual data points in Figure 5. This figure indicates that most transverse slab cracking occurs in a vertical band between -2 and $+2$. Thus, as fatigue damage approaches 1 [i.e., as $\log_{10}(n/N)$ approaches 0], the likelihood of transverse slab cracking increases greatly. The range of values results because of variations in material properties, erosion, traffic estimations, and other factors.

Linear and nonlinear regression procedures were used to try to fit a model through the data. Although there was a large scatter of data, a reasonable model was fit through the

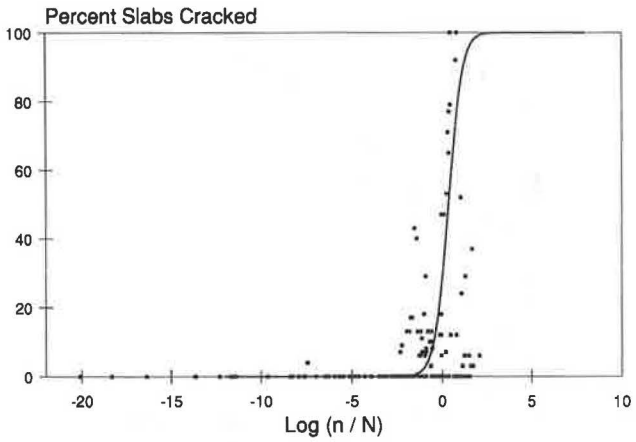

FIGURE 5 Percent slab cracking as a function of accumulated fatigue damage.

data. The model, which is plotted in Figure 5, is given as follows:

$$P = \frac{1}{0.01 + 0.03 * [20^{-\log(n/N)}]} \quad (5)$$

where P is the percent of slabs cracked and n is the actual number of 18-kip ESAL applications at the slab edge.

Equation 5 fits the data fairly well and is in the classical S-shaped curve, which is thought of as representing actual distress development. As such, the curve meets the required boundary conditions (i.e., zero slab cracking for zero fatigue damage and 100 percent slab cracking for infinite fatigue damage). The curve comes close to meeting the theoretical 50 percent slab cracking for $\Sigma\ n/N = 1$.

A sensitivity analysis was performed using the equation for several key pavement design inputs. Figure 6 shows slab cracking as a function of 18-kip lane (not edge) ESAL applications for different shoulder types. The section with a tied PCC shoulder (20 percent stress load transfer efficiency assumed) and the section with a widened outside traffic lane and AC shoulder exhibit little, if any, transverse cracking. However, the section with the AC shoulder displays a significant amount of transverse cracking.

Figure 7 shows a similar sensitivity analysis for joint spacing. The positive influence of shorter slabs on reducing transverse cracking is clearly evident. The reduction in slab cracking between 20- and 15-ft slabs is significant, but additional benefit is also seen in reducing the joint spacing to 10 ft.

Figure 8 shows a sensitivity analysis of the transverse cracking model with respect to slab thickness. The 8-in. slab exhibits extensive slab cracking early in its life. Increasing the slab thickness from 8 to 10 in. has an enormous effect on reducing the development of fatigue cracking. Likewise, an increase in slab thickness from 10 to 12 in. reduces the amount of transverse slab cracking to essentially zero.

Although the cracking model employs a mechanistic approach to the development of transverse cracking, there are other factors currently not incorporated (e.g., thermal coefficient of expansion and friction from the base) that also are believed to contribute to cracking.

Transverse Joint Spalling

Joint and corner spalling is defined as any type of fracture or deterioration of the transverse joints, excluding corner breaks. Only medium- and high-severity joint spalling is included in the prediction models.

A wide range of designs are included in this evaluation. The combined data base used in the evaluation provided 262 data points for JPCP and 280 data points for JRCP. The data were cleaned to remove any sections that had unusual load transfer mechanisms (e.g., ACME devices) or that were constructed using ineffective joint forming methods (e.g., Unitube joint inserts). This procedure was followed because these devices may actually contribute to joint spalling, and new construction does not use the devices.

The data represent a wide range of climates from the major climatic zones across the United States: wet-freeze, wet-nonfreeze, dry-freeze, and dry-nonfreeze. The only exception

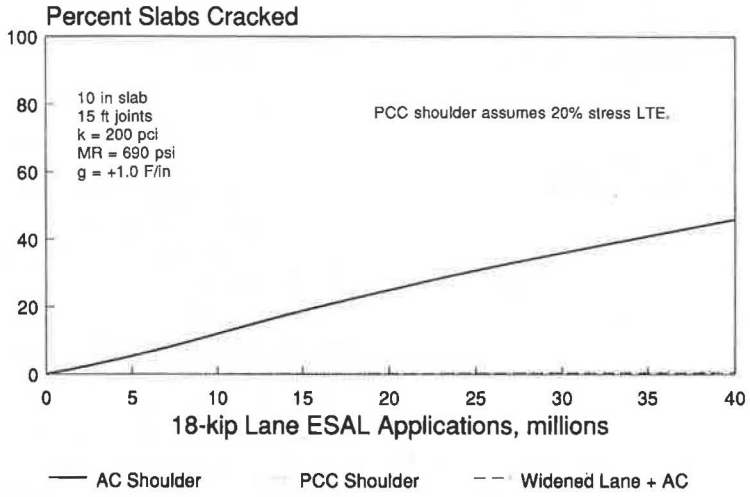

FIGURE 6 Sensitivity of JPCP cracking model to shoulder type.

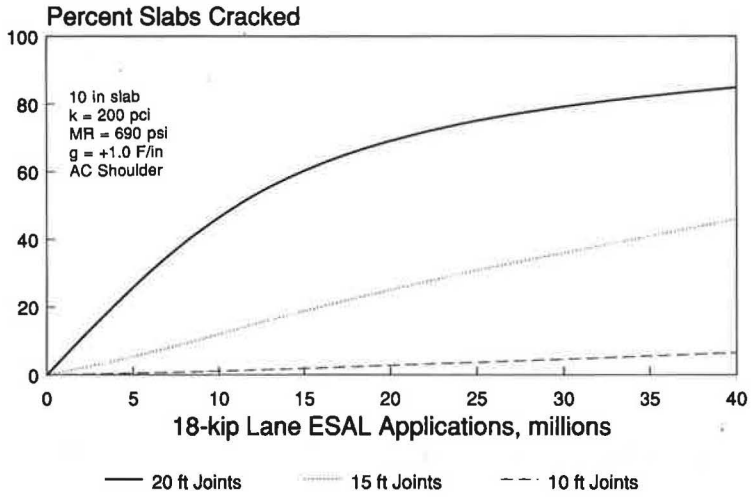

FIGURE 7 Sensitivity of JPCP cracking model to joint spacing.

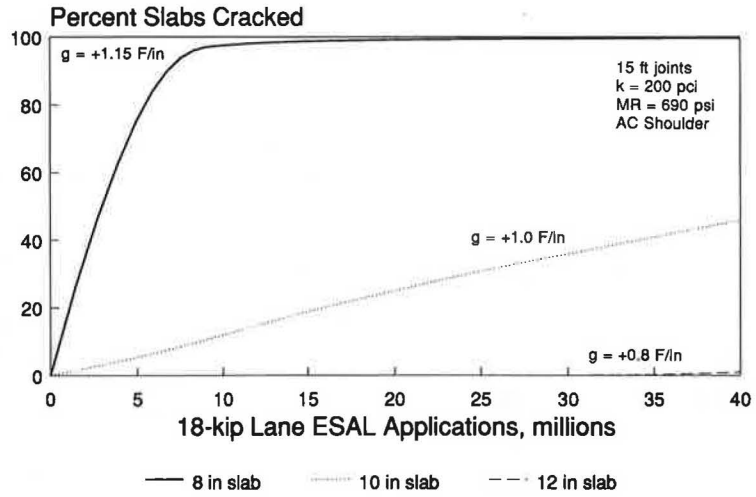

FIGURE 8 Sensitivity of JPCP cracking model to slab thickness.

was that there were no JRCP sections located in dry-nonfreeze areas.

Prediction models were developed separately for JPCP and JRCP. Extensive efforts to develop a single model for joint spalling were unsuccessful. One reason may be that most of the joint spalling for JPCP was of medium severity; few joints had high-severity spalling. JRCP sections, however, had a much greater proportion of joints exhibiting high-severity joint spalling.

JPCP Joint Spalling Model

The final joint spalling model for JPCP is given as follows:

$$\text{JTSPALL} = \text{AGE}^{2.178} * (0.0221 + 0.5494\,\text{DCRACK} - 0.0135\,\text{LIQSEAL} - 0.0419\,\text{PREFSEAL} + 0.0000362\,\text{FI}) \quad (6)$$

where

JTSPALL = number of medium-high joint spalls per mile;
AGE = age since original construction (years);
DCRACK = 0 if no D-cracking exists, 1 if D-cracking exists;
LIQSEAL = 0 if no liquid sealant exists in joint, 1 if liquid sealant exists in joint;
PREFSEAL = 0 if no preformed compression seal exists, 1 if preformed compression seal exists; and
FI = freezing index (degree-days below freezing).

Statistics:

R^2 = 0.59,
SEE = 15 joints/mi, and
n = 262.

The sensitivity of the model is shown in Figures 9 and 10. Figure 9 shows the average effect that joint sealants have on

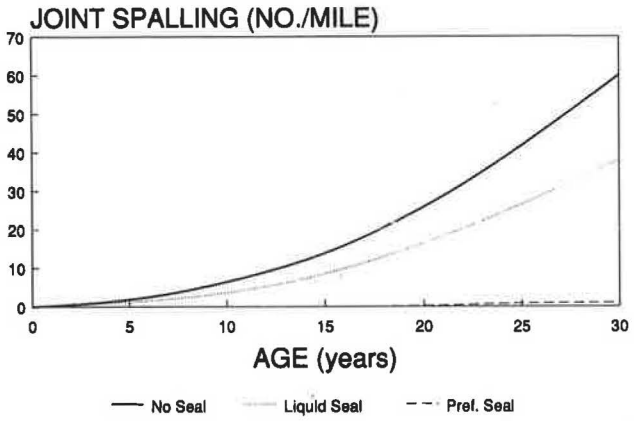

FIGURE 9 Sensitivity of JPCP spalling model to joint sealant type.

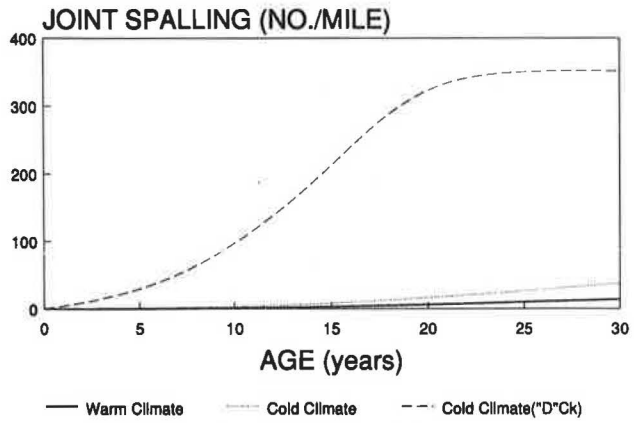

FIGURE 10 Sensitivity of JPCP spalling model to climate.

a JPCP in a cold climate (FI = 400, no D-cracking). Having a liquid joint sealant reduces the amount of spalling by nearly 50 percent over a 30-year period. A preformed sealant reduces the amount of joint spalling to essentially zero over a 30-year period. Because incompressibles are believed to be the major cause of joint spalling, it appears that preformed sealants are capable of keeping incompressibles from infiltrating the joints for a significant period of time.

Figure 10 shows the dramatic effect of D-cracking on joint spalling. It also shows the effect of a warm climate (FI = 0) and a freezing climate (FI = 400) on the development of joint spalling.

JRCP Joint Spalling Model

The final joint spalling model for JRCP is given as follows:

$$\text{JTSPALL} = \text{AGE}^{4.1232} * (0.00024 + 0.0000269\ \text{DCRACK} + 0.000307\ \text{REACTAGG} - 0.000033\ \text{LIQSEAL} - 0.0003\ \text{PREFSEAL} + 0.00000014\ \text{FI}) \quad (7)$$

where REACTAGG is 0 if no reactive aggregate exists and 1 if reactive aggregate exists.

Statistics:

$R^2 = 0.47$,
SEE = 13 joints/mi, and
$n = 280$.

A sensitivity of the model is shown in Figure 11. This figure shows the average effect that joint sealants have on a JRCP in a cold climate (FI = 400, no D-cracking). Having a liquid joint sealant reduces the amount of spalling by about 11 percent over a 30-year period. However, a preformed sealant reduces the amount of joint spalling to essentially zero over the same 30-year period.

Present Serviceability Rating

The performance data were also used to develop predictive models for the mean panel PSR. The models were of the form where PSR is the dependent (y) variable and pavement distress types are the independent (x) variables.

The prediction of panel PSR ratings has been modeled several ways in the past. The original PSR equation from the AASHO Road Test was based on both roughness and distress (*12*). Many other models have been developed solely on the basis of roughness (*13*) or visual distress (*14*).

The best way to predict PSR is using roughness. However, a PSR model based only on key distress types is useful in mechanistic-empirical design of pavements to approximately relate physical deterioration (that can be estimated using other models) to serviceability, or user response.

PSR prediction models were developed both for JPCP and for JRCP. Although all measured types of distress were initially considered, only three key distress types proved significant: joint faulting, joint deterioration (spalling), and trans-

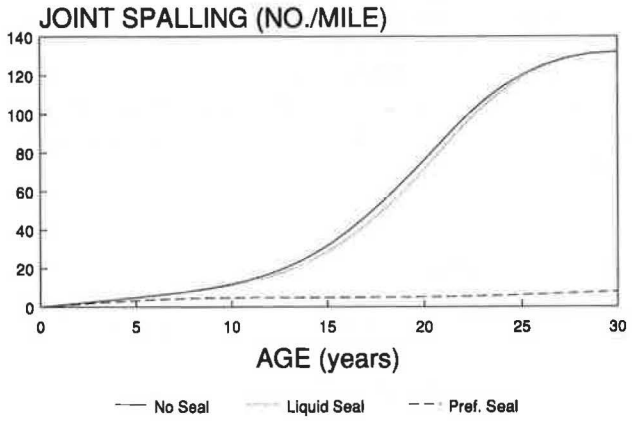

FIGURE 11 Sensitivity of JRCP spalling model to joint sealant type.

verse cracking. The presence of full-depth patching was also of significance and was included in the equations.

The models for each pavement type are as follows:

Jointed Plain Concrete Pavements

$$PSR = 4.356 - 0.0182\,TFAULT - 0.00313\,SPALL - 0.00162\,TCRKS - 0.00317\,FDR \quad (8)$$

where

PSR = mean panel rating of pavement (0 to 5 AASHTO scale),
TFAULT = cumulative transverse joint faulting (in./mi),
SPALL = number of deteriorated (medium- and high-severity) transverse joints per mile,
TCRKS = number of transverse cracks (all severities) per mile, and
FDR = number of full-depth repairs per mile.

Statistics:

$R^2 = 0.58$,
SEE = 0.31 (units of PSR), and
$n = 282$.

Jointed Reinforced Concrete Pavements

$$PSR = 4.333 - 0.0539\,TFAULT - 0.00372\,SPALL - 0.00425\,MHTCRKS - 0.000531\,FDR \quad (9)$$

where MHTCRKS is the number of medium- and high-severity cracks per mile.

Statistics:

$R^2 = 0.64$,
SEE = 0.37 (units of PSR), and
$n = 434$.

The values of R^2 and SEE are similar to those of the original PSR models developed at the AASHO Road Test (*12*).

Examination of the PSR models indicates that transverse joint faulting has the greatest effect on reducing the PSR. Spalling, transverse cracking, and full-depth repairs have a much smaller effect on reducing PSR.

The primary limitation of these models is that they do not include either all distress types or long-wavelength roughness, such as would be caused by settlements or heaves. In fact, the relatively low R^2 values and high standard errors clearly indicate that other sources of variation in PSR exist.

These models are not intended to be used to predict PSR (or PSI) in place of roughness, because it can be demonstrated that measured roughness is the best way to predict serviceability. These models are intended for use in predicting serviceability when only key distress types are available. Even then, the models should be used with caution, recognizing their limitations.

EXAMPLE USE OF MODELS

An example application of the models for checking concrete pavement designs is presented in Table 2. It is assumed that the thickness of the slab has been determined using an agency-approved method and that the various design features (such as load transfer, base type, and AC shoulder) have been selected in accordance with agency policy or procedures. The inputs needed for each model are listed in Table 2 under the appropriate heading.

The original design was tested using the models. In the first iteration, the level of faulting (0.14 in.) and the amount of slab cracking (88 percent) resulting from the analysis are both unacceptable. The amount of joint spalling is acceptable, however, and the estimate of the overall serviceability is marginal for this pavement type and traffic loading.

A target design value for the faulting of nondoweled pavements is 0.07 in., whereas a target design value for slab cracking is 10 to 15 percent of the slabs cracked. To accomplish this, several design changes were made to the original design: tied PCC shoulders were added, the joint spacing was shortened to 15 ft, and an open-graded permeable base with edge drains was included. This revised design was again tested using the models in the second iteration. The result of this change is that joint faulting is marginally acceptable, although slab cracking is still somewhat high. Joint spalling is still acceptable and the PSR is quite adequate. However, because of the faulting and cracking, the design requires specific features to restrict the development of these distresses: 1.25-in. dowel bars to control the faulting and a 10-in. slab to reduce the cracking. This design change was tested using the models in the third iteration, and the results indicate that the design is more than adequate.

SUMMARY

Several performance prediction models for concrete pavements have been presented. A combination of theory, mechanistic variables, and field performance data was used in the development of the models. Because of the large data base of in-service pavements from which they were developed, these models are believed to possess the most comprehensive and accurate prediction capability to date.

The models can be useful in checking pavement designs for the development of faulting, cracking, joint spalling, and serviceability loss. They can also be used to develop design guidelines for joint load transfer, widened traffic lanes, tied shoulders, permeable bases, and many other design variables. However, the models must be used with care and not extended beyond the inference space from which they were developed.

ACKNOWLEDGMENTS

This paper is based on the results of a research project conducted by ERES Consultants, Inc., for FHWA. The authors are grateful for the assistance provided by Ying-Haur Lee and Ricardo Salsilli of the University of Illinois in the development of the models. In addition, the direction and guidance pro-

TABLE 2 EXAMPLE APPLICATION OF MODELS TO CHECK CONCRETE PAVEMENT DESIGN

Initial Design

9 in JPCP — No Dowels
Asphalt-Treated Base (k = 200) — Cold Climate
20-ft joint spacing — Fine-grained subgrade

Faulting Inputs			Cracking Inputs			Spalling Inputs		
ESAL	=	10 million	ESAL	=	10 million	AGE	=	20 years
CON	=	0.65	n	=	0.5 million (5% * 10 million)	DCRACK	=	None
AVJSPACE	=	20 ft				FI	=	600
ALPHA	=	0.000006 strain/°F	MR_m	=	700 psi (28-day modulus of rupture)	Sealant Type	=	Hot-poured rubberized (liquid)
TRANGE	=	75 °F						
e	=	0.00015 strain shrinkage	g	=	1.05 °F / in (thermal gradient)			
E_c	=	4,200,000 psi						
P	=	9000 lb	P	=	9000 lb (wheel load)			
a	=	5.64 in						
KSTAT	=	200 psi/in	JTSPACE	=	20 ft			
THICK	=	9 in	Shlder Type	=	AC			
μ	=	0.15	KSTAT	=	200 psi/in			
Base Type	=	4 in asphalt treated	ES	=	341 psi (edge stress, from reference 9)			
FI	=	600						
DRAIN	=	None						
EDGESUP	=	AC Shoulder	N	=	46,610 applications (from Eq. 4)			
STYPE	=	Fine-grained soil						

Iteration No. 1 - original design

Predicted Faulting = 0.14 in (from Eq. 2)
Predicted Cracking = 88 percent of the slabs (from Eq. 4)
Predicted Spalling = 20 joints/mile (from Eq. 6)
Predicted PSR = 3.2 (from Eq. 8 after converted to consistent units)

Design not adequate; faulting and slab cracking unacceptable.

Iteration No. 2 - PCC shoulders, 15 ft joint spacing, permeable base with edge drains

Predicted Faulting = 0.09 in
Predicted Cracking = 25 percent of the slabs (assuming 45 percent stress load transfer across the shoulder)
Predicted Spalling = 20 joints/mile
Predicted PSR = 3.7

Design marginally adequate for faulting, inadequate for slab cracking.

Iteration No. 3 - 1.25 in dowel bars, 10 in slab

Predicted Faulting = 0.03 in
Predicted Cracking = 0.1 percent of the slabs
Predicted Spalling = 20 joints/mile
Predicted PSR = 4.1

Based upon the results of this iteration, the design, as revised, is acceptable.

vided by Roger M. Larson, FHWA contract manager, is gratefully acknowledged.

REFERENCES

1. *AASHTO Guide for Design of Pavement Structures, 1986.* AASHTO, Washington, D.C., 1986.
2. A. J. van Wijk. *Rigid Pavement Pumping: Volume 1—Subbase Erosion; Volume 2—Economic Modeling.* Final Report. FHWA, U.S. Department of Transportation, Sept. 1985.
3. A. J. van Wijk, J. Larralde, C. W. Lovell, and W. F. Chen. Pumping Prediction Model for Highway Concrete Pavements. *Journal of Transportation Engineering, ASCE*, Vol. 115, No. 2, March 1989.
4. A. J. van Wijk. *Purdue Economic Analysis of Rehabilitation and Design Alternatives for Rigid Pavements: A User's Manual for PEARDARP.* Final Report. FHWA, U.S. Department of Transportation, Sept. 1985.
5. M. I. Darter, J. M. Becker, M. B. Snyder, and R. E. Smith. *NCHRP Report 277: Portland Cement Concrete Pavement Evaluation System—COPES.* TRB, National Research Council, Washington, D.C., Sept. 1985.
6. K. W. Heinrichs, M. J. Liu, M. I. Darter, S. H. Carpenter, and A. M. Ioannides. *Rigid Pavement Analysis and Design.* Report FHWA-RD-88-068. FHWA, U.S. Department of Transportation, July 1989.
7. K. D. Smith, A. L. Mueller, M. I. Darter, and D. G. Peshkin. *Performance of Jointed Concrete Pavements, Volume II—Evaluation and Modification of Concrete Pavement Design and Analysis Models.* Report FHWA-RD-89-137. FHWA, U.S. Department of Transportation, Aug. 1990.
8. A. M. Ioannides, M. R. Thompson, and E. J. Barenberg. Westergaard Solutions Reconsidered. In *Transportation Research Record 1043*, TRB, National Research Council, Washington, D.C., 1985.
9. M. I. Darter. *Design of Zero-Maintenance Plain Jointed Pavement, Volume 1—Development of Design Procedures.* Report FHWA-RD-77-111. FHWA, U.S. Department of Transportation, April 1977.
10. R. F. Benekohal, K. T. Hall, and H. W. Miller. Effect of Lane Widening on Lateral Distribution of Truck Wheels. In *Transportation Research Record 1286*, TRB, National Research Council, Washington, D.C., 1990.
11. M. I. Darter. *A Comparison Between Corps of Engineers and ERES Consultants, Inc. Rigid Pavement Design Procedures.* U.S. Air Force SAC Command, Aug. 1988.
12. *Special Report 61E: The AASHO Road Test, Report 5—Pavement Research.* HRB, National Research Council, Washington, D.C., 1962.
13. M. I. Darter and E. J. Barenberg. *Zero-Maintenance Pavements: Results of Field Studies on the Performance Requirements and Capabilities of Conventional Pavement Systems.* Report FHWA-RD-76-105. FHWA, U.S. Department of Transportation, 1976.
14. K. T. Hall, J. M. Connor, M. I. Darter, and S. H. Carpenter. *Rehabilitation of Concrete Pavements, Volume III—Concrete Pavement Evaluation and Rehabilitation System.* Report FHWA-RD-88-073. FHWA, U.S. Department of Transportation, July 1989.

Publication of this paper sponsored by Committee on Rigid Pavement Design.